Macromolecules

ARTICLE

pubs.acs.org/Macromolecules

Counterion Dynamics in Polyester−Sulfonate Ionomers with Ionic Liquid Counterions

Gregory J. Tudryn,[†] Wenjuan Liu,[†,⊥] Shih-Wa Wang,[‡] and Ralph H. Colby[†,*]

[†]Department of Materials Science and Engineering [‡]Department of Chemical Engineering The Pennsylvania State University, University Park, Pennsylvania 16802, United States

ABSTRACT: Conventional sodium cations (Na^+) in sulfonated polyester ionomers were replaced with ammonium-based ionic liquid counterions. Counterion dynamics were measured by dielectric spectroscopy and linear viscoelastic response via oscillatory shear. Ion exchange from sodium counterions to ionic liquid counterions such as tetramethylammonium and tetrabutylammonium showed an order of 10^4 increase in conductivity compared with sodium counterions, primarily attributed to weaker ionic interactions that lower the glass transition temperature. Electrode polarization was used in conjunction with the 1953 Macdonald model to determine the number density of conducting counterions and their mobility. Conductivity and mobility exhibit Vogel−Fulcher−Tammann (VFT) temperature dependences and both increased with counterion size. Conducting counterion concentrations showed Arrhenius temperature dependences, with activation energy reduced as counterion size increased. When ether−oxygen was incorporated into the mobile cation structure, self-solvating ability notably increased the conducting ion concentration. Weakened ion pairing interactions prove favorable for fundamental design of single-ion conductors for actuators, as ionic liquid counterions can provide both larger and faster strains, required by such electro-active devices.

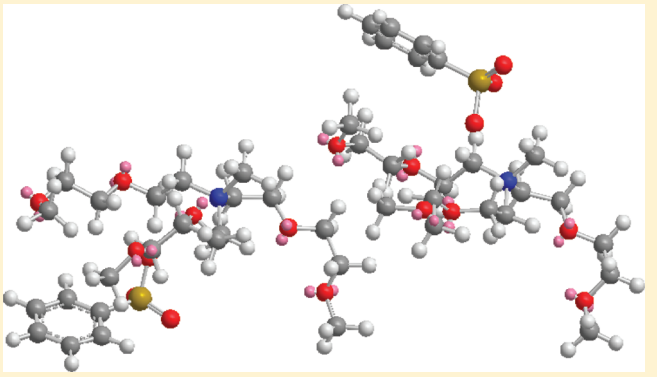

1. INTRODUCTION

Electrolyte systems play an integral part in ionic devices and energy storage applications. Facile ion transport through electrolytes allows efficient charging, energy storage and discharging. Improvements being pursued to replace liquid electrolytes with polymer can reduce battery mass and improve flexibility and safety. Solvent-free polymer electrolytes, however, have limited conductivity due to the inability of ions to dissociate in low dielectric constant media.[1−4] Poly(ethylene oxide), (PEO) with a dissolved lithium salt was among the first candidate polymer electrolyte materials for advanced rechargeable lithium batteries due to the ability of ether-oxygen to disrupt salt aggregates and solvate Li^+.[5−8]

In contrast to salt systems, single-ion conductors are built by covalently attaching the anion to the polymer to make an ionomer.[9] The anion consequently does not respond to the field on a reasonable time scale and the transference number for the counterion is extremely close to unity. This design circumvents problems with anions polarizing at electrodes and allows simpler analysis of ion motion than PEO/salt systems. Ionomeric single-ion conductors need low glass transition temperature, as ion motion is coupled with segmental motion of the ionomer.[10−13] With Li^+ counterions, such materials might be candidates for electrolytes in batteries, but the room temperature conductivity is presently too low with existing ionomers. A major factor in low ionomer conductivity is ion associations. Ions tend to pair and associate with other pairs to form multiplets and aggregates which do not participate in ionic conductivity, thus lowering conducting ion density. Associated ion pairs are known to act as physical cross-links.[14,15] The resulting slowed polymer segmental dynamics are reflected in an increase in the glass transition temperature as ions are added to the polymer, often as large as 8 K per mol % of ionic monomers.[9]

This study intends to use the ability of ionic liquids to disrupt aggregate formation and improve ionomer segmental dynamics and conductivity. Room temperature ionic liquids prevent effective packing into a stable crystal lattice through delocalized charge, steric hindrance, and asymmetry of anion−cation pairs.[16−19] In our study, ammonium based ionic liquid cations are exchanged in place of sodium cations on a polyester-sulfonate ionomer while retaining a consistent 1.5 polymer backbone ether oxygens per cation, and six ester groups per cation. The ability of ionic liquids to reduce pair associations is explored in this study as a function of cation size and functionality, to identify desirable characteristics for enhanced conducting ion density and mobility in ionomers.

With larger counterions, the conductivity can be improved considerably and such materials are potentially useful for systems

Received: November 8, 2010
Revised: March 13, 2011
Published: April 08, 2011

ACS Publications © 2011 American Chemical Society

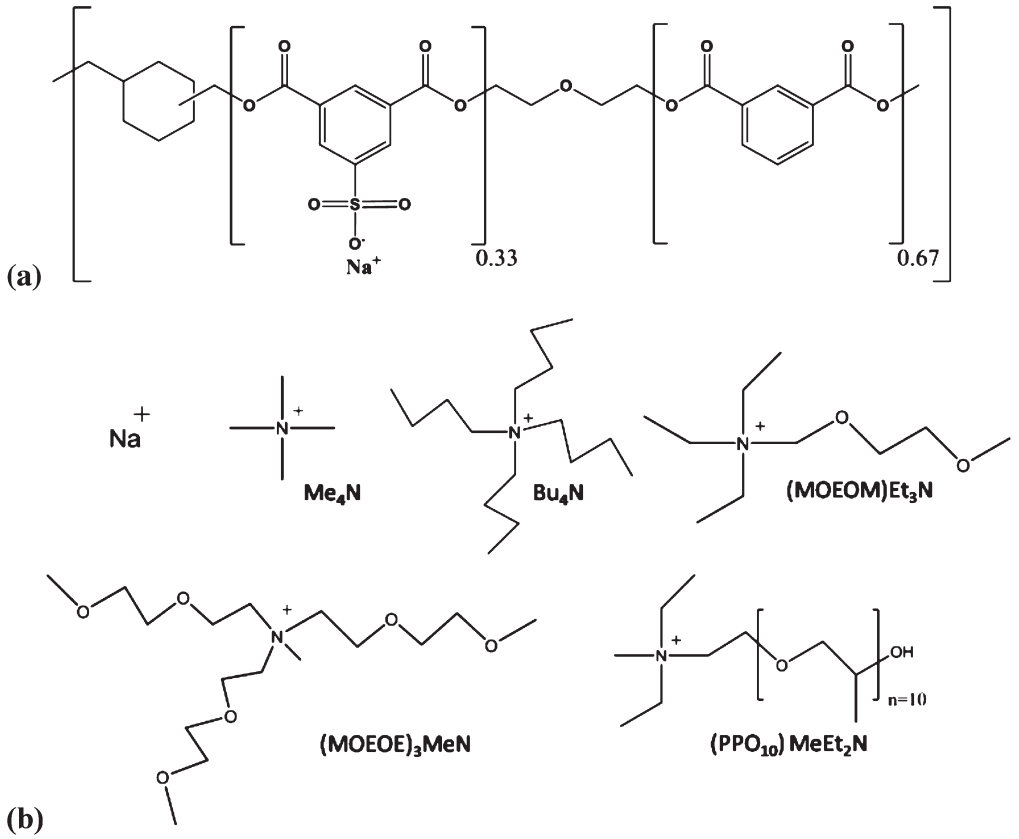

Figure 1. (a) Polyester-sulfonate ionomer structure, with ratio of sulfonated and neutral phthalates determined by NMR, M_n = 8000 g/mol, theoretical ion content 4.43 × 10^{20} cm^{-3} for the Na ionomer. (b) Cationic counterion structures: sodium, tetramethylammonium, tetrabutylammonium, (2-methoxyethoxymethyl)triethylammonium, tris[2−2(methoxyethoxy)ethyl]methylammonium, [poly(propylene oxide)]methyldiethylammonium are shown, left to right, top to bottom, respectively. Note, MALDI−TOF shows that $(PPO_{10})MeEt_2N$ has a Gaussian distribution around $n = 10$ with $5 < n < 15$.

such as thin film actuators using ionic electro-active polymers. This study uses ammonium-based ionic liquid cations in a sulfonated polyester ionomer with a constant sulfonate anion content to observe dielectric, structural, and mechanical impacts of weakly coordinating counterions. Fundamentally, ionic liquids also provide more volume change upon macroscopic polarization under an applied field compared to smaller ions, which is favorable for use in electro-active devices such as ionic actuators.[16,20−26]

2. EXPERIMENTAL TECHNIQUES

2.1. Ion Exchange and Purification. Sulfonated polyester with sodium counterions (Figure 1a) received from Sigma-Aldrich was dissolved in deionized water and purified using Amicon cellulose dialysis membranes with molecular weight cutoff of 3000 g/mol. The ionomer was exchanged to the acid state using sulfonated styrene-divinyl benzene ion-exchange resin, then immediately titrated to between pH 7−8 using ionic liquid hydroxides (Figure 1b) from Sigma-Aldrich, TCI, and Solvent Innovation-GmbH. Samples were then further dialyzed to remove any impurities using Amicon PLAC membranes of cutoff 1000 g/mol until the dialyzate reached the conductivity of the inlet deionized water stream (~0.7 μS/cm). Molecular weight (M_n = 8000 g/mol from manufacturer) was unaffected by the ion-exchange process, as checked by aqueous SEC ($M_w/M_n \approx 2$). Efficiency of cation exchange was assessed to >98% using inductively coupled plasma to measure atomic emission spectra of sulfur and residual sodium on a Perkin-Elmer Optima 5300.

2.2. *Ab Initio* Calculations. To support this study, *ab initio* calculations were employed to determine counterion diameter, interaction energies of ion states, and dipole moment of ion pairs. Calculations were performed using density functional theory methods using the Gaussian 03 software package. Exchange and correlation were included using the hybrid-GGA B3LYP functional. Counterion diameter was determined by average cross-sectional size of cations after full equilibrium. Dipole moments of polar solvents and interaction energy of polar solvents with ions agree with vapor phase data for the basis set used.

2.3. Thermal Characterization. Purified materials were analyzed using a TA Q1000 differential scanning calorimeter (DSC) under ultra high purity nitrogen purge at 50 mL/min. Samples of approximately 4.0 mg were heated to 403 K for 30 min, cooled to 183 at 10 K/min and held isothermally for 5 min before ramping to 403 at 10 K/min. Glass transition temperature, T_g, was identified as the midpoint of the shift in heat capacity.

2.4. X-ray Scattering. Small-angle X-ray scattering (SAXS) data were collected using pinhole collimation and a Mar CCD detector on Beamline 12-BM at the Advanced Photon Source at Argonne National Laboratories, Lemont, IL, under beam conditions of 18KeV and 100 mA. SAXS data were reproduced on a Molecular Metrology instrument using a Cu target (λ = 1.54 Å) and a gas phase two-dimensional area proportional counter. Scattering intensity was measured under high vacuum with operating conditions of 0.67 mA and 45 kV with a sample to detector distance of 150 cm.

2.5. Linear Viscoelasticity. Mechanical response was studied using a Rheometric Scientific ARES-LS1 Rheometer with 7.9 mm diameter parallel plates at temperatures more than 40 K above T_g and 2.0 mm diameter parallel plates at temperatures near T_g. Samples were vacuum

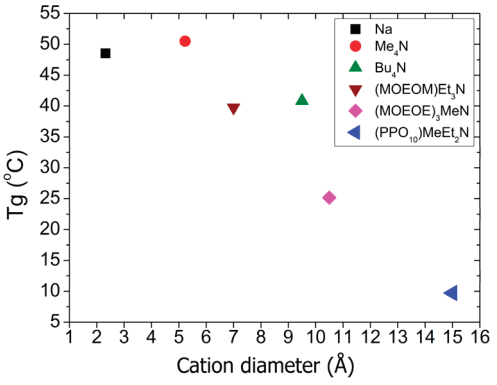

Figure 2. Calorimetric glass transition temperatures of the polyester ionomer as a function of counterion size (values listed in Table 1) estimated from average cation cross sections from *ab initio* (±0.5 Å).

molded at $T = T_g + 80$ K for approximately 4 h to remove voids and water, then heated under nitrogen for >4 h on the instrument plates at $T = T_g + 80$ K for precise geometry and proper contact. Small strain amplitudes corresponding to linear viscoelastic (LVE) response were verified using strain amplitude sweeps at fixed frequency. Time−temperature superposition was found to work well for all ionomers studied, and was used to construct master curves.

2.6. Dielectric Relaxation Spectroscopy (DRS). A Novocontrol GmbH Concept 40 broadband dielectric spectrometer applying a.c. voltage with amplitude 0.1 V was used to study linear electrical response of all ionomers. Purified ionomers were heated at $T_g + 80$ K for 4 days under vacuum on polished brass electrode disks of 30 mm diameter to ensure complete contact and removal of water and voids. This helps eliminate artificially high conductivity in hygroscopic samples. Sample geometry was dictated by 100 μm Teflon spacers with a top electrode of 20 mm diameter applied after drying the sample with thickness exceeding 100 μm.

Before measurements, samples were annealed in the instrument at 423 K for 2 h under nitrogen to allow further drying (≤0.7 wt % by Karl Fischer titration). Isothermal frequency sweeps from 10^7 to 10^{-2} Hz in 10 K steps down to 253 K measured conductivity and dielectric response of the ionomer at high frequency, conductivity and dielectric constant at intermediate frequency and electrode polarization at low frequency, all with precise temperature control, within ±0.05 K.

3. RESULTS AND DISCUSSION

3.1. Thermal Properties. Figure 2 correlates glass transition temperature with counterion size. While T_g is known to increase with ion content due to the presence of physical cross-links, this effect is significantly reduced with larger counterions.[9,27,28] Physical cross-links in ionomers are viewed as dipolar interactions between ion pairs, where two or more dipoles effectively negate each other and form a stable quadrupole, or primary aggregate. With constant ion content, our polyester-sulfonate ionomers show T_g decreasing as counterion size increases. This is caused by two effects. Larger counterions associate less, forming fewer and weaker physical cross-links that raise the T_g of ionomers. Larger counterions also act as plasticizers, further lowering T_g.[28−30]

3.2. X-ray Scattering. To verify large cations reduce physical cross-linking, or ionic aggregation, we turn to X-ray scattering, a common tool for identifying ionic aggregates.[9,31−35] Ionic aggregation can be identified through the wavevector q of ionomer peaks, where $q = (4\pi/\lambda)\sin(\theta/2)$, with X-ray wavelength, λ and scattering angle, θ. Typical ionomers with similar ion contents have been reported to show peaks near $q = 0.15-0.2$ Å^{-1} corresponding to Bragg spacing of $d = 2\pi/q \approx 3$ nm between ion aggregates.[9,31−35] Figure 3 shows the X-ray results for our polyester ionomers shifted vertically for clarity. The sodium ionomer has the most scattering in the 0.02 Å^{-1} < q < 0.17 Å^{-1} range, suggesting that the ionomer with Na counterions has the most extensive ion aggregation. The absence of a specific peak suggests there is a range of interaggregate spacings covering 3−30 nm. Me_4N and Bu_4N also show significant ion aggregation though not as much as Na. (MOEOM)Et_3N shows only a hint of ion aggregation (small ionomer peak centered at 0.06 Å^{-1}) while the two largest counterions show no evidence of any ion aggregation in SAXS. A reduction in ionic aggregates for large cations is also reflected in the T_g values reported in Table 1; suggesting larger counterions form fewer (and weaker) aggregates. This ability is important for improved segmental dynamics necessary for ion conduction, and less ionic aggregation will also result in faster LVE relaxation.[9,15,28,29,36]

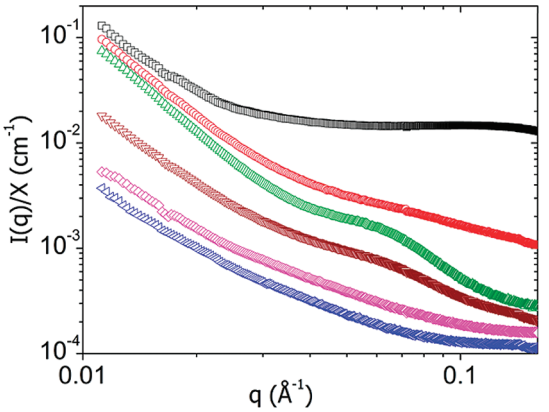

Figure 3. Synchrotron small-angle X-ray scattering curves divided by shift factor, x, for clarity. From top to bottom: (black square) Na ($x = 1$); (red dot) Me_4N ($x = 1$); (green triangle pointing up) Bu_4N ($x = 1.25$); (brown triangle pointing down) (MOEOM)Et_3N ($x = 4$); (purple diamond) (MOEOE)$_3$MeN ($x = 6.67$); (blue triangle pointing left) (PPO_{10})$MeEt_2$N ($x = 6.67$).

Table 1. Cation Average Cross-Section Diameter from *ab Initio* Calculations and T_g Determined from DSC

cation	cation diameter (Å)	T_g (midpoint) (K)
Na	2.3	321.7
Me_4N	5.2	323.7
Bu_4N	9.5	314.0
(MOEOM)Et_3N	7.0	312.9
(MOEOE)$_3$MeN	10.5	298.3
(PPO_{10})$MeEt_2$N	15.0	282.9

The ionomers with Bu_4N and (MOEOM)Et_3N counterions show microphase separation of ionic aggregates from the polymer, with a peak/shoulder at $q \approx 0.06$ Å^{-1}, indicating a well-defined spacing between ion domains of $2\pi/q \approx 10$ nm. These two most hydrophobic ions have a poor ability to form quadrupoles due to steric effects and are simultaneously less compatible with the polymer than either of the smaller ions (Na and Me_4N) or the larger the ions containing 6−10 ether oxygens.

3.3. Linear Viscoelastic Properties. Mechanical response probed by small amplitude oscillatory shear is useful for observing the impact of associating ion pairs, or aggregates acting as physical cross-links between chains.[14,15,36−38] Figure 4 shows the master curves for these ionomers over a broad range of moduli

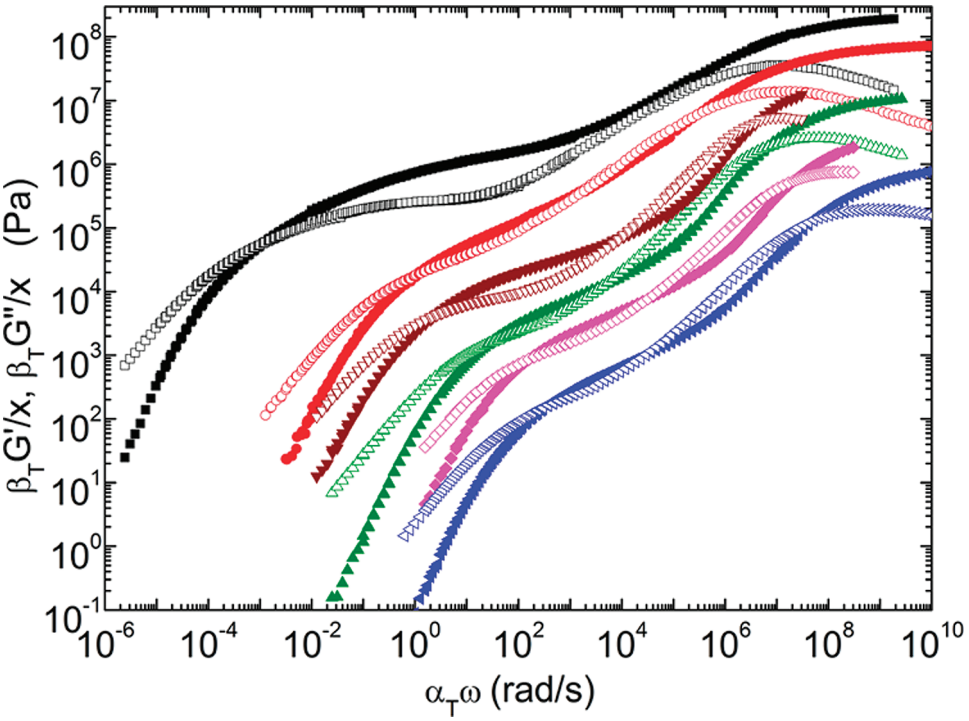

Figure 4. Linear viscoelastic properties via oscillatory shear of polyester-sulfonate ionomers containing ionic liquid counterions, closed symbols represent storage modulus G′, and open symbols represent loss modulus, G''. Master curves referenced to 100 °C are then divided by vertical shift factor, x for clarity. From top to bottom: (black square) Na (x = 1); (red dot) Me_4N (x = 10); (green triangle pointing up) Bu_4N (x = 100); (brown triangle pointing down) (MOEOM)Et_3N (x = 33); (purple diamond) $(MOEOE)_3MeN$ (x = 250); (blue triangle pointing left) $(PPO_{10})MeEt_2N$ (x = 1000).

and angular frequencies, constructed using time−temperature superposition. The sodium ionomer was seen to have significantly longer time scales for terminal response, presumably because the small accessible sodium-sulfonate ion pairs associate more than those of the larger counterions, which is also reflected in the higher T_g (Figure 2) and the more aggregated SAXS profile (Figure 3). Decrease of terminal response time follows the plasticizing trend which is caused by reduction of physical cross-links from fewer and weaker associations of ion pairs.[15,28,29,37,38]

Aqueous size exclusion chromatography showed identical chain length for our ionomer with different counterions, suggesting the extension of the rubbery plateau with smaller ions is due to the presence of associations between ion pairs acting as physical cross-links. The effective monomer time, τ_0, can be taken as the reciprocal of the frequency of the high frequency peak in G'' and the low frequency crossing of G' and G'' determines the terminal relaxation time, τ_{rep}.[39] These two fundamental time scales allow us to quantify the viscoelastic delay and correlate it with counterion type. Table 2 shows a clear correlation between the cation size and the ratio τ_{rep}/τ_0, indicating that the larger counterions have very little ion aggregation with similar τ_{rep}/τ_0. Me_4N has significant ion aggregation, with τ_{rep}/τ_0 5−15 times larger and Na has extensive ion aggregation, with τ_{rep}/τ_0 3000−10000 times larger.

The presence of this feature follows trends seen in reversible networks with physical cross-links which show prolonged viscoelastic relaxation for systems with associating groups versus those without them.[14,36] This cross-correlation, combined with glass transition temperature and SAXS observations suggests that the associations seen in the larger cations are fewer and/or weaker, indicating that the use of ionic liquid cations is successfully reducing aggregate formation. The successful disruption of stable aggregates through the use of cation selection will also impact conductive properties and give further insight into the type of ionic liquid preferred for electroactive devices.[18,20−26,40]

Table 2. Linear Viscoelastic Time Scales at 100 °C[a]

cation	cation diameter (Å)	τ_0 (s)	τ_{rep} (s)	τ_{rep}/τ_0
Na	2.3	7.6×10^{-8}	840	1.1×10^{10}
Me_4N	5.2	5.4×10^{-8}	1.0	1.9×10^{7}
Bu_4N	9.5	1.5×10^{-8}	0.034	2.2×10^{6}
(MOEOM)Et_3N	7.0	1.0×10^{-7}	0.38	3.6×10^{6}
$(MOEOE)_3MeN$	10.5	5.2×10^{-9}	0.0063	1.2×10^{6}
$(PPO_{10})MeEt_2N$	15.0	9.7×10^{-10}	0.0027	2.8×10^{6}

[a] τ_0 represents the monomer time as the inverse of the higher frequency at the maxima in G'' and τ_{rep} is evaluated as the inverse of the low frequency where G' crosses G'', representing terminal response.

3.4. Dielectric Relaxation Spectroscopy.

3.4.1. Polymer Dynamics. Polymer segmental relaxations in dielectric spectroscopy are observed as cooperative dipole relaxations along the polymer backbone under an applied field. At a specific time scale and temperature the polymer has the ability to relax a segment, which is observed as a peak in the dielectric loss (the imaginary portion of the complex dielectric function) in the frequency domain.[41] In ion containing systems, this relaxation is often small in comparison to other dielectric loss events, i.e., conductivity, and is often difficult to resolve. One technique used in this field to remove conductivity is manipulation of the Kramers−Kronig transform to yield the dielectric loss without

dx.doi.org/10.1021/ma102547q |*Macromolecules* 2011, 44, 3572–3582

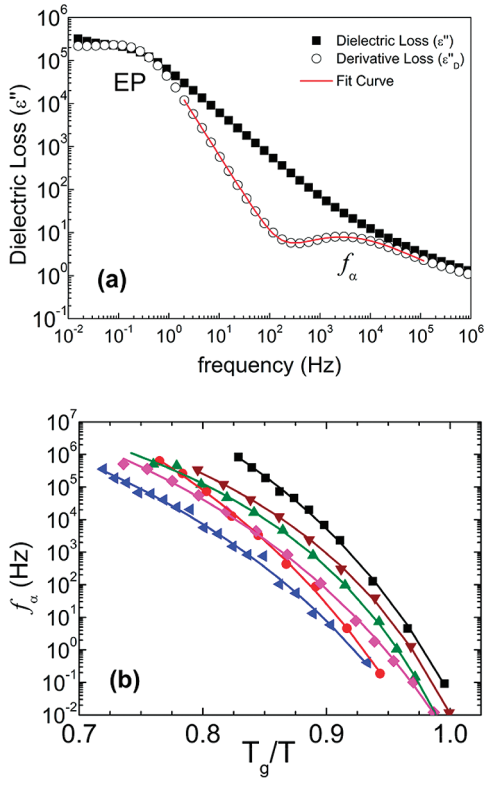

Figure 5. (a) Dielectric loss spectra and derivative loss spectra fit to the sum of a power law for EP and the derivative form of the HN function[42,43,62] for (MOEOM)Et_3N at 80 °C. (b) α-relaxation frequency maxima of the polyester−sulfonate ionomers with varied cations as a function of temperature normalized by T_g.

the purely lossy conduction. Derivative loss similarly removes conductivity, calculated from the frequency-dependent dielectric constant $\varepsilon'(f)$ in the following form.[42,43]

$$\varepsilon_{der}(f) = -\frac{\pi}{2}\frac{\partial \varepsilon'(f)}{\partial(\ln f)} \quad (1)$$

Figure 5a compares $\varepsilon''(f)$ and $\varepsilon_{der}(f)$ at a temperature where conduction and electrode polarization dominate the response. The large increase at low frequencies is electrode polarization (EP), while the peak at higher frequencies in $\varepsilon_{der}(f)$ corresponds to the α (segmental) relaxation. To quantify the peak α-relaxation frequency, the derivative loss is fit over a range of temperatures using the appropriate form[42,43] of the Havriliak−Negami function,[41] (eq 2) while simultaneously fitting EP to a simple power law function (1 Hz to 100 Hz in Figure 5a) to curve resolve the α-relaxation from electrode polarization.

$$\varepsilon^*_{HN}(f) = \frac{\Delta\varepsilon}{[1+(if/f_{HN})^a]^b} \quad (2)$$

$\Delta\varepsilon$ is the relaxation strength, f_{HN} is the frequency related to the peak maximum, and a and b are shape parameters ($a = b = 1$ yields a simple Debye relaxation). To obtain the frequency maximum in the dielectric loss indicative of the α-relaxation time, it is necessary to use the following conversion:[41]

$$f_\alpha = f_{HN}\left(\sin\frac{a\pi}{2+2b}\right)^{1/a}\left(\sin\frac{ab\pi}{2+2b}\right)^{-1/a} \quad (3)$$

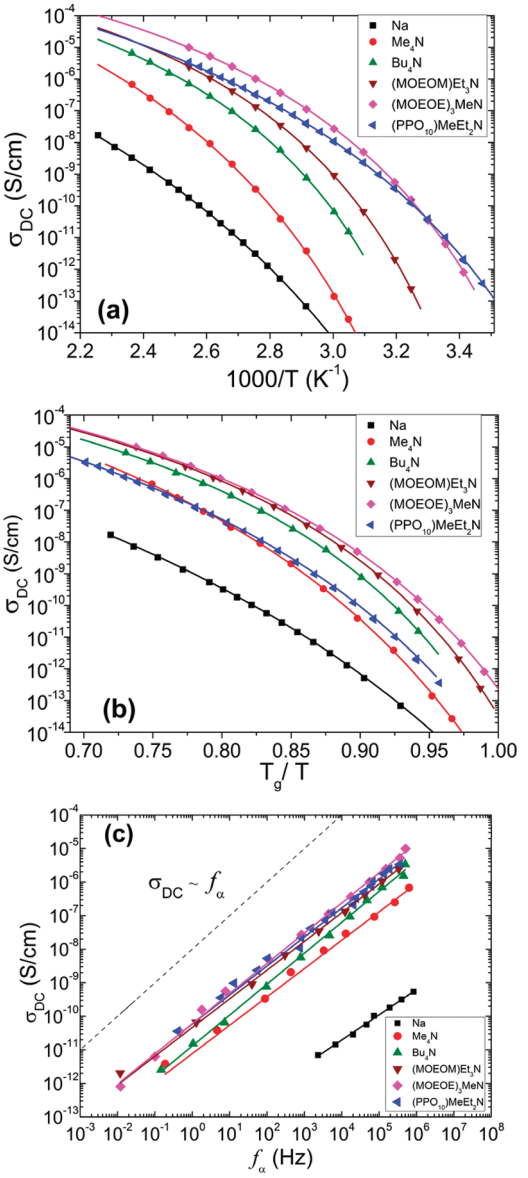

Figure 6. (a) DC ionic conductivity of polyester-sulfonate ionomers with different counterions as a function of temperature with VFT fits to eq 4 as solid curves, with parameters listed in Table 3. (b) DC ionic conductivity of sulfonated polyester ionomers as functions of ion type and temperature normalized by T_g. (c) DC conductivity of the polyester−sulfonate ionomers with varied cations as a function of their respective α-relaxation times.

Figure 5a shows an example fit using the derivative form of the HN function. Figure 5b shows α-relaxation frequencies calculated from eq 3 as a function of reciprocal temperature normalized by the DSC T_g. It should be noted that these values appropriately extrapolate to 0.01 s^{-1} as temperature approaches the glass transition ($T_g/T = 1$); coupled with strong curvature in Figure 5b, this identifies f_α as the segmental relaxation of the polymer associated with the glass transition.[41,44]

3.4.2. Ionic Conductivity. DC conductivity, σ_{DC}, is observed as the in-phase conductivity, $\sigma'(\omega)=\varepsilon''(\omega)\varepsilon_0\omega$, independent of frequency for an approximate three decade range. As noted by the trends in T_g and linear viscoelasticity, polymer dynamics are more facile through the incorporation of ionic liquid cations. Figure 6a

displays the impact of faster segmental motion through a ca. 10^4 increase in conductivity with increased counterion size, with ether oxygen-containing counterions having the highest conductivity. Figure 6a also shows all ion types exhibit Vogel−Fulcher−Tammann (VFT) behavior, eq 4, which signifies ion motion is coupled with segmental relaxation above the Vogel temperature, T_0.

$$\sigma_{DC} = \sigma_\infty \exp\left(\frac{-B}{T - T_0}\right) \quad (4)$$

T_0 and B (inversely related to fragility) can be extracted from fitting the VFT behavior (eq 4), where dynamics at temperatures below T_0, approximately $T_g - 50$ K, lack the free volume necessary for ions to migrate.[41,44] Figure 6b normalizes temperature by the DSC T_g, showing that segmental motion is not the sole source of improved conductivity. The conductivity at fixed T_g/T increases with ion size except for the largest cation, where the long PPO tail lowers ion mobility.

Ionic conduction relies on polymer segmental motion, so suppression of T_g is important for improvements in conductivity. Figure 6c correlates the DC conductivity with the α-relaxation frequency for the six different counterions. The Debye−Stokes−Einstein equation expects ion motion to be strongly coupled to polymer segmental motion, with DC conductivity proportional to α-relaxation frequency.

$$\sigma_{DC} \propto f_\alpha \quad (5)$$

Instead of this perfect correlation, the data in Figure 6c suggest

$$\sigma_{DC} \propto f_\alpha^{0.86 - 0.90} \quad (6)$$

similar to previous observations on sulfonate ionomers based on poly(ethylene oxide).[44,45] As expected, the studied ionomers have DC conductivity strongly correlated to, but not perfectly coupled to, segmental motion. The collapse of conductivity to a single curve indicates that the segmental motion in larger cations is similar, while the small sodium ion has reduced conductivity in comparison. This is likely due to the propensity to form aggregates, seen in trends in T_g, SAXS, and linear viscoelasticity, and is reflected in the conducting ion density which will be discussed in the next section.

To further investigate, conductivity must be resolved into its components. Use of ionomers, or single-ion conductors, allows the application of the Macdonald/Coelho electrode polarization model to determine the temperature dependent conducting ion content p and mobility μ, whose product multiplied by ion charge, e, determines the conductivity of single-ion conductors.

$$\sigma_{DC} = \mu p e \quad (7)$$

In the next few sections we model electrode polarization to determine p and μ.

3.4.3. Conducting Ion Number Density. Electrode polarization occurs at low frequencies and is noticeable by polarized ions at the electrodes reducing the field, causing increased capacitance and dielectric constant, and lower conductivity.[13,44] Figure 7 shows the two observable time scales used for measurement of ion transport properties, the time scales for conduction (τ_σ), and electrode polarization (τ_{EP}):

$$\tau_\sigma \equiv \frac{\varepsilon_s \varepsilon_0}{\sigma_{DC}} \quad (8)$$

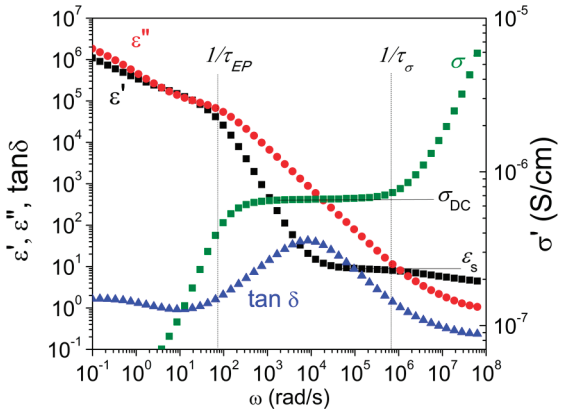

Figure 7. Polyester-sulfonate ionomer with Me_4N cation response to applied AC field at 150 °C. DC conductivity σ_{DC} is noted as the frequency independent section in the real portion of complex conductivity, σ' (green square). The static dielectric constant, ε_s is taken as the value of the real portion of the complex dielectric function ε' (black square) before electrode polarization starts. Low frequencies show electrode polarization analogous to charging a macroscopic capacitor where dielectric storage, ε' and loss ε'' (red dot) increase by several orders of magnitude. The peak of the loss tangent tan $\delta \equiv \varepsilon''/\varepsilon'$ (blue triangle) gives the geometric mean of the time scales of conductivity and electrode polarization, $(\tau_\sigma \tau_{EP})^{1/2}$.

$$\tau_{EP} \equiv \frac{\varepsilon_{EP} \varepsilon_0}{\sigma_{DC}} \quad (9)$$

Where ε_s is the measured static relative permittivity of the sample before electrode polarization, ε_0 is the permittivity of vacuum and ε_{EP} is the significantly increased permittivity after electrode polarization. The Macdonald model treats electrode polarization as a simple Debye relaxation and the loss tangent is fit to obtain the time scales in eqs 8 and 9.[13,46]

$$\tan \delta = \frac{\omega \tau_{EP}}{1 + \omega^2 \tau_\sigma \tau_{EP}} \quad (10)$$

Figure 8 shows the angular frequency, $\omega = 2\pi f$, dependence of the loss tangent fit to eq 10, resulting in determination of τ_σ and τ_{EP}. The model then determines the number density of conducting ions p and their mobility μ from τ_{EP} and τ_σ

$$p = \frac{1}{\pi l_B L^2}\left(\frac{\tau_{EP}}{\tau_\sigma}\right)^2 \quad (11)$$

$$\mu = \frac{e L^2 \tau_\sigma}{4 \tau_{EP}^2 kT} \quad (12)$$

where

$$l_B = \frac{e^2}{4\pi\varepsilon_0 \varepsilon_s kT} \quad (13)$$

is the Bjerrum length, L is the sample thickness, e is the charge that is identical for all monovalent cations, k is the Boltzmann constant and T is absolute temperature. Equation 11 shows that the number density of conducting ions is determined from the square of the magnitude of electrode polarization ($\tau_{EP}/\tau_\sigma = \varepsilon_{EP}/\varepsilon_\sigma$) while the mobility is reciprocally related to the product of the magnitude and time scale of electrode polarization. The time scale τ_{EP} is proportional to electrode spacing L, as expected by

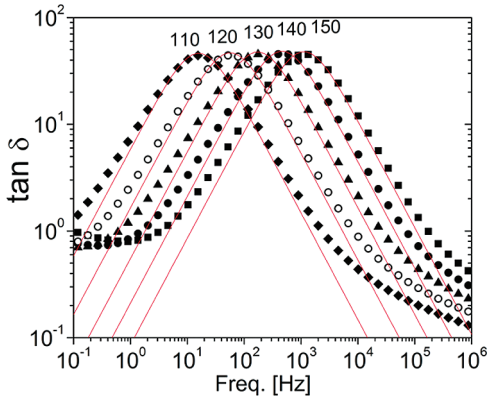

Figure 8. Frequency dependence of loss tangent tan $\delta \equiv \varepsilon''/\varepsilon'$ for the ionomer with Me_4N counterions at five temperatures (°C). Solid curves are fits of the loss tangent to eq 10. Key: (■) 150 °C; (●)140 °C; (▲)130 °C; (○)120 °C; (♦)110 °C.

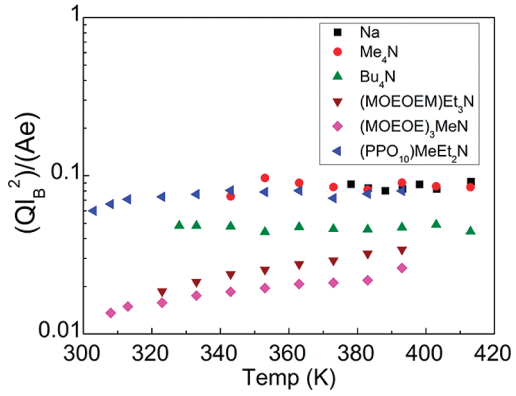

Figure 9. Electrode polarized counterions per squared Bjerrum length comparison for the ionomer with different counterions. All values are small compared with unity, indicating that our 0.1 V amplitude is within the linear limit of applied electric field.

the Macdonald model[46] and observed for polyester-sulfonate ionomers based on poly(ethylene oxide).[13,44] This indicates the number density of conducting ions p and their mobility μ are material properties that are independent of L.

An important concern for use of the Macdonald model is electrode material-dependent results[47] and surface roughness.[48] Results show strong dependence on oxide layer formation, most notably aluminum electrodes exhibit significantly less electrode polarization.[47] Oxidation strongly impacts the strength of polarization, as the insulating layer may prevent counterions from moving close to the charges on the metal electrode. Polished mirror-finish brass, stainless steel or gold are suitable electrode materials for use with the Macdonald model; we utilize the former for all of our studies of electrode polarization in single-ion conductors. We have compared three types of electrodes with the ionomers in this paper and several that we previously reported.[10,44,45] We consistently find that our polished mirror-finish stainless steel electrodes give slightly weaker electrode polarization than polished mirror-finish brass, with conducting ion content p typically a factor of 0.6 smaller with polished mirror-finish stainless steel electrodes. On the other hand, sputtering gold onto the polished mirror-finish brass increases the magnitude of electrode polarization, with p typically a factor of 2 larger; most likely this is simply reflecting an increase in electrode surface area from sputtered gold. We have settled on polished mirror-finish brass electrodes, which give reproducible results (relative error within ±20% for p).

A material property relevant for electroactive actuation is τ_{EP}/L, obtained from eq 12.

$$\frac{\tau_{EP}}{L} = \sqrt{\frac{e\tau_\sigma}{4\mu kT}} = \frac{1}{\mu}\sqrt{\frac{\varepsilon_s\varepsilon_0}{4pkT}} \tag{14}$$

Here we used eqs 7 and 8. For fast actuation, ion-conducting membranes need to be thin (small L) have high mobility μ of conducting ions, and a high conducting ion content p.

Actuation can be modeled as an equivalent resistor-capacitor circuit, with the time scale for polarization (or charging) $\tau_{EP} = RC$, where R is the resistance and C the capacitance of the equivalent circuit. The actuation is created on time scale τ_{EP} by a buildup of conducting ions in the Stern layer (within the Debye length of the electrode). The charge Q built up within the Stern layer is directly proportional to the applied voltage V, as $Q = CV = \tau_{EP}V/R$. With the resistance $R = L/(\sigma_{DC}A)$, where A is the electrode surface area, we have a simple relation for the charge accumulation per unit of electrode surface area (charge density).

$$\frac{Q}{A} = \frac{\tau_{EP}}{L}V\sigma_{DC} \tag{15}$$

The material property τ_{EP}/L multiplied by the conductivity σ_{DC} determines the charge density at the electrode. Combining eqs 14 and 15 writes the charge density in terms of the number density of conducting ions and the dielectric constant.

$$\frac{Q}{A} = Ve\sqrt{\frac{\varepsilon_s\varepsilon_0 p}{4kT}} \tag{16}$$

In order to increase strain in actuators, we need to increase the charge density of polarizing ions, which requires membranes with large dielectric constant ε_s and high number density of conducting ions p.

The above is based upon linear response theory, whereas real actuators likely rely on nonlinear polarization of ions. The Macdonald model assumes that the buildup of ions near the electrode is sufficiently small that they do not interact with other ions near the electrode. High concentrations of ions would suggest that application of the Macdonald model should fail,[49] however the theory is valid as long as there are few ions simultaneously conducting (so that even fewer are actually polarizing). Nonlinear electrode polarization will occur when the polarizing ions start to interact with each other — when they are separated by the Bjerrum length on the electrode surface (where their Coulomb repulsion is the thermal energy).

The relevant dimensionless parameter is (from eq 15)

$$\frac{Ql_B^2}{Ae} = \frac{\tau_{EP}V\sigma_{DC}l_B^2}{Le} = Vl_B^2\sqrt{\frac{\varepsilon_s\varepsilon_0 p}{4kT}} = \frac{eV}{kT}\sqrt{\frac{pl_B^3}{16\pi}} < 1 \tag{17}$$

Figure 9 shows all data have $0.01 < Ql_B^2/(Ae) < 0.1$, suggesting that our applied voltage amplitude of 0.1 V is well within linear response for all of our ions. The onset voltage for nonlinear effects in electrode polarization will depend on the particular ionomer and counterion, through the conducting ion content and dielectric constant (Bjerrum length).

After verification of linearity, we look at the temperature dependence of conducting ion density, Figure 10, which is Arrhenius (eq 18). Fitting to the Arrhenius equation is done with the stoichiometric ion content set as the parameter for the high temperature limit.[13,44] This assumption elucidates the trend

that the ionomers with larger counterions have reduced activation energy, with values listed in Table 3.

$$p = p_\infty \exp\left(-\frac{E_a}{RT}\right) \quad (18)$$

One important conclusion from Figure 10 is that there is a small fraction of ions simultaneously participating in conduction. Sodium has of order 10^{-3} fraction of ions simultaneously contributing to conductivity, as observed for other sodium sulfonate polyesters,[13] while the largest counterions have the fraction of conducting ions of order 10^{-2}. Fractions of counterions conducting of order 10^{-2} have been reported for lithium sulfonated polyesters,[44] but these had 13 or more ether oxygens per counterion. It is crucial to realize that in fact all ions participate in conduction; there is an exchange between various ion states (isolated pairs, triples, quadrupoles, etc.) and at the time scale τ_σ the DC conductivity is reached, beyond which counterion mean-squared displacement is diffusive, meaning that all counterions participate in ion-conduction. However, the relevant level of counterion participation in the mean-field solution of the Poisson−Boltzmann equation for the double layer is of that in any *instantaneous snapshot*. While obvious, this point has been confused in the literature.[50]

Another vital point is that both MD simulation[51] and various spectroscopies[52−55] often see significant fractions of ions (of order half) that are apparently free in their "snapshots." However, a truly free counterion needs to be more than the Bjerrum length away from its sulfonate partner, which is a vanishingly small population. Most counterions are in some sense paired (coupled) with their sulfonate anion, but that ion state is not necessarily a contact pair (or exists only a fraction of the time in direct contact). Our current hypothesis is that the conducting counterions are in a triple ion state[56−58] (two counterions coupled with the same sulfonate) that exchanges the extra counterion with a nearby pair on the time scale faster than τ_σ (when all counterions access all states and participate equally in conduction) but this view is speculative and difficult to test.

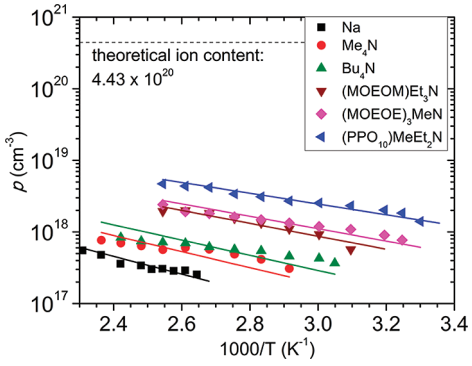

Figure 10. Conducting ion number density from the electrode polarization model (eq 11). Lines show Arrhenius temperature dependence (eq 18) using activation energy as the sole fitting parameter, with intercepts fixed (at $T = \infty$) at the calculated total ion content of $p_\infty = 4.43 \times 10^{20}$ cm^{-3}.

The trend of reduced activation energy in Figure 10 and Table 3, or lowered ion dissociation energy, with larger ions is also seen in other systems with varied sizes of monovalent alkali metal ions,[11,13,59] but is exaggerated here by our use of ionic liquid cations. Note that the sodium counterion has the lowest conducting ion density due to the tendency of the ions to stay trapped in more aggregated states and only able to respond to the applied electric field at much lower frequencies. The larger ions have been noted to be in a less aggregated state, but also as ions are made significantly larger, the center to center distances of charges lengthens which reduces the energy required to provide conducting ions. This follows predictions by Coulomb's law indicating larger cation−anion separation distances have lower energy required to separate the pair $E \sim -e^2/d$, where $-e$ is the anion charge and $+e$ is the cation charge and d is the charge separation distance.

Another notable feature is that the presence of ether oxygen on conducting cations increases conducting ion number density. The ability of ether oxygen to break up associated ion pairs acting as cross-links is also seen through trends in glass transition temperature, and shorter linear viscoelastic terminal time of the ionomers containing large counterions. Ether oxygens on the cation incorporate a self-solvating effect which stabilizes isolated pairs from association and increases conducting ion content, which contribute to dielectric constant and conductivity, respectively. This is a particularly strong self-solvation effect because our ionomer only has 1.5 EO/cation, whereas our parallel study of polyurethane−carboxylate ionomers[60] has 26 EO/cation with greatly reduced effects of incorporating ether oxygens into the cation.

3.4.4. Dielectric Constant. Static dielectric constant is the frequency independent value of dielectric storage at arbitrarily long time scales, a material property of the sample between electrodes. Since other contributions to dielectric storage, such as electrode polarization convolute this value, it is calculated using eq 8 from the measured σ_{DC} and τ_σ obtained from fitting EP to eq 10, yielding the low frequency dielectric constant before the onset of electrode polarization and macroscopic charge accumulation. Dielectric constant in ionomers (and all liquids) typically scales inversely with temperature due to thermal randomization,[61] which can be described as a broadened distribution of dipole orientations as temperature increases. The dielectric

Table 3. VFT Parameters for DC Conductivity and Counterion Mobility and Arrhenius Activation Energy for Conducting Ion Density with Fixed Theoretical Ion Content, $p_\infty = 4.43 \times 10^{20}$ cm^{-3}

	DC conductivity			mobility			ion density
cation	σ_∞ (S/cm)	B	T_0 (K)	μ_∞ (cm^2/(V s))	B	T_0 (K)	E_a (kJ/mol)
Na	0.0024	2400	245	0.0022	1800	260	23.8
Me_4N	1.51	2600	246	1.05	2070	255	21.5
Bu_4N	0.10	1620	256	0.44	1520	256	20.3
$(MOEOM)Et_3N$	0.18	1540	250	0.38	1650	241	17.3
$(MOEOE)_3MeN$	2.11	1570	233	0.16	1370	235	16.6
$(PPO_{10})MeEt_2N$	0.19	2030	213	0.17	1810	214	14.4

dx.doi.org/10.1021/ma102547q |*Macromolecules* 2011, 44, 3572–3582

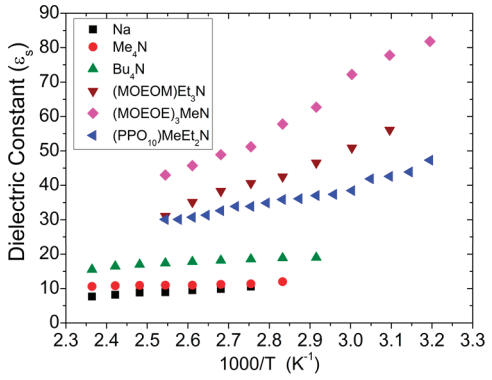

Figure 11. Temperature dependence of ionomer static dielectric constant, for the six counterions. Decreasing dielectric constant as temperature increases follows the Onsager 1936 prediction based upon thermal randomization.[61]

Table 4. Dipole Moments from *ab Initio* Equilibrated Ion Pairs at 0 K Compared to Values Calculated from Static Dielectric Constant Using eq 19, Assuming All Ions Are Isolated Ion Pairs

cation	*ab initio* pair dipole moment (D)	pair dipole moment from ε_s (D)
Na	7.8	6.5−7.5
Me_4N	11	13.8−14.3
Bu_4N	13	17.5−18.0
$(MOEOM)Et_3N$	11	25−30
$(MOEOE)_3MeN$	9.0	30−35
$(PPO_{10})MeEt_2N$	14	24.0−26.5

constant of a neutral version of our ionomer (without sulfonated phthalates) should be near 5 (relatively large for polymers), while the observed dielectric constant of these ionomers in Figure 11 indicates other contributions to dielectric constant, such as dipole moments from isolated ion pairs. Because of counterion size, ionic liquids have larger anion−cation equilibrium separation distance providing a larger dipole moment than a typical ion pair with an alkali metal cation. The tendency to form associated pairs is also disrupted due to ion pair asymmetry and steric hindrance, which also inhibit crystallization of ionic liquids. Breaking aggregates into isolated pairs is expected to increase the static dielectric constant due to the presence of more pairs acting as dipoles that can rotate/align under an applied field.[44]

For further understanding of ion pair states in the system, the dielectric constant is used to estimate the dipole moment of the pairs present which are contributing to dielectric constant. To determine the effective average ion pair dipole moment, we assume the dipole moments of associated pairs (quadrupoles and larger aggregates) are negligible compared to the number and magnitude of the dipole moment of isolated ion pairs, while triple ions and free ions have insignificant populations. It is reasonable to assume the only significant contribution to dielectric constant is from ions in the isolated ion pair state. While some pairs are associated in symmetric structures with quite small dipoles, others exist as separated pairs, and we estimate an average value of effective pair dipole moment.

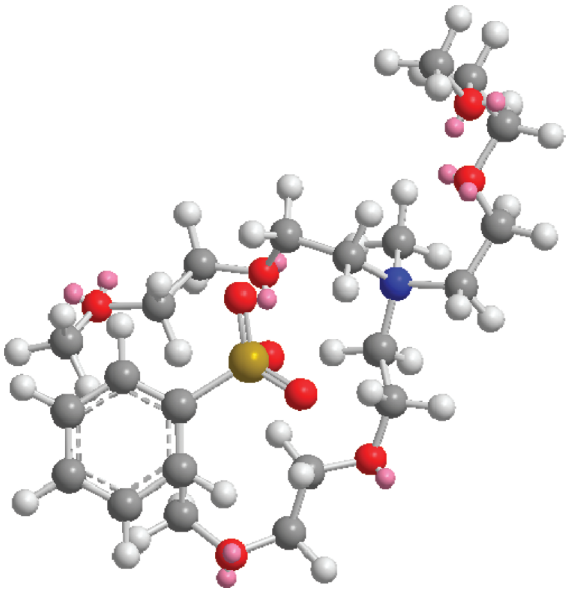

Figure 12. Atomistic illustration of an equilibrated ion pair consisting of counterion $(MOEOE)_3MeN$ with self-solvating capability (blue, nitrogen; red, oxygen; gray, carbon; white, hydrogen; pink, lone pairs on oxygen) with benzenesulfonate (yellow, sulfur).

Use of the Onsager model, eq 19, determines the average value of effective ion pair dipole moment, μ_{pair}.[61]

$$\mu_{pair} = \sqrt{\frac{(9\varepsilon_0 kT)(\varepsilon_s - \varepsilon_\infty)(2\varepsilon_s + \varepsilon_\infty)}{\nu\varepsilon_s(\varepsilon_\infty + 2)^2}} \qquad (19)$$

Here ε_0 is the permittivity of vacuum, ε_∞ is the high frequency permittivity of the sample (allowing full atomic polarization but no molecular motion, here taken to be $\varepsilon_\infty = 2.1$) and $\nu = 4.4 \times 10^{20}\text{cm}^{-3}$ is the total number density of counterions. Table 4 compares the values of μ_{pair} from the Onsager analysis to *ab initio* calculations for contact pairs at 0 K in vacuum. With the exception of Na^+, which shows the most aggregation, the average dipole moments from eq 19 are consistently larger than *ab initio* results, indicating that the real dipoles are significantly larger than those of the contact pairs. Ion pairs can have larger separations than a contact pair and this effect is seen with $(MOEOE)_3MeN$, shown in Figure 12. This effect is less dramatic for the largest counterion $PPO_{10}MeEt_2N$ (Table 4 and Figure 11) presumably because the long PPO tail still allows strong ion interactions, since the methyl diethyl face of this ammonium is quite exposed, although this counterion unfortunately never equilibrates in our *ab initio* calculations for contact pair energy. Figure 11 and Table 4 indicate an optimum counterion size, with significant ether oxygen self-solvation, as $(MOEOE)_3MeN$ (Figure 12) has the highest dielectric constant and largest effective ion pair dipole moment.

3.4.5. Conducting Ion Mobility. Figure 13a shows that reduced counterion dissociation energy has an observable increase in ionic mobility, μ at all temperatures with the trend that larger ions have higher mobility. Since ion motion is coupled with segmental dynamics,[44] the same mobility data are plotted against T_g/T in Figure 13b. Mobility increases with counterion size and eventually saturates at an optimal size where Bu_4N, $(MOEOM)Et_3N$, and $(MOEOE)_3MeN$ have similar mobilities. This indicates that mobility increases with the reduction of

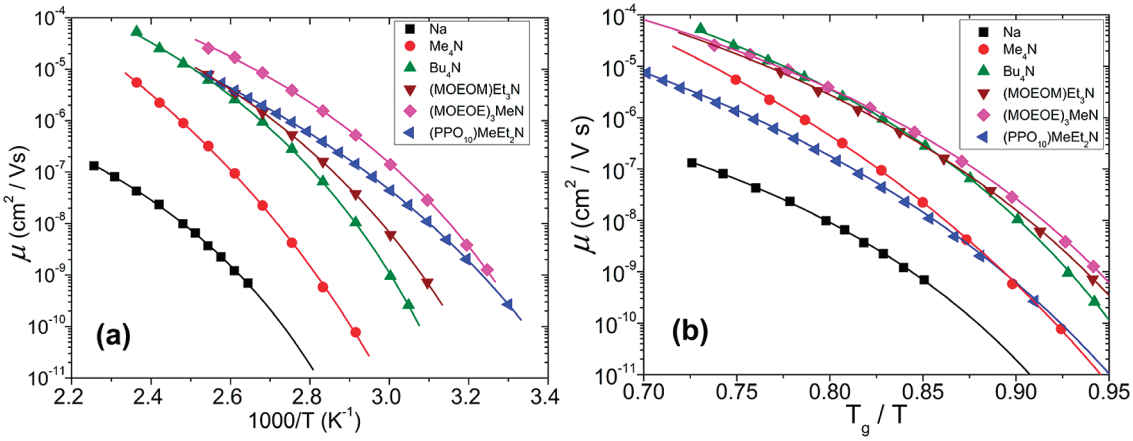

Figure 13. (a) Mobility of conducting counterions of polyester-sulfonate ionomers as functions of temperature and ion type. (b) Mobility of conducting counterions of polyester-sulfonate ionomers as functions of ion type and temperature normalized by T_g. VFT parameters listed in Table 2, with fits shown as solid curves.

associated pairs, which we observe these ions have few of in comparison to Me_4N and Na. It is key to note that the largest ion has an excessively long PPO tail which helps plasticize the ionomer to the largest extent, but is effectively too long and lowers counterion mobility when compared using T_g/T.

4. SUMMARY

Counterion dynamics in a sulfonated polyester ionomer were studied via exchange to various cation moieties. Sodium ions were replaced with ionic liquid cations and thermal, rheological, and dielectric properties showed enhancements for electro-active applications. Trends in T_g, conductivity, conducting ion density, mobility, and dielectric constant provide insight into desirable counterion properties.

First, large sterically hindering counterions are necessary for proper disruption of associated ion pairs, causing inability of multiple ion pairs to pack due to steric effects or asymmetry of dipoles, which results in suppressed T_g. The disruption of aggregates, or physical cross-links, is also observed in SAXS as a decrease in scattering in the ionomer peak region. Linear viscoelasticity provides terminal response times that are shortened with larger cations which disrupt physical cross-links.

Second, ether-oxygen functionality on cations provides self-solvating characteristics which enhance ionic conduction through other means than suppressed glass transition temperature. Application of the Macdonald model for electrode polarization reveals improvements in conducting ion density and mobility. A note must be made that while ions with large side groups may appropriately lower T_g and improve conducting ion content and mobility, excessive size (oligomeric counterions) eventually hinders ionic mobility.

In electro-active devices, ionic liquid cations allow increased performance through tuning of intrinsic material properties by using the ability of large counterions to plasticize and disrupt ion associations without additional solvent. Those large ions should presumably also generate more strain in electrode polarization, relevant to actuators.

AUTHOR INFORMATION

Corresponding Author

*E-mail: rhc@plmsc.psu.edu.

Present Address

[⊥]The Dow Chemical Company, Midland, Michigan 48674, United States.

ACKNOWLEDGMENT

This material is based upon work supported in part by the U.S. Army Research Office under Grant No. W911NF-07-1-0452 Ionic Liquids in Electro-Active Devices (ILEAD) MURI. Use of the Advanced Photon Source at Argonne National Laboratory was supported by the U.S. Department of Energy, Office of Science, Office of Basic Energy Sciences, under Contract No. DE-AC02-06CH11357. The authors thank Byeongdu Lee and Seonke Seifert for providing time on beamline 12-BM at the Advanced Photon Source and Alicia Castagna for derivative spectra advice. We thank James Runt, Michael Janik, Timothy Long, Sean Ramirez, and Qiming Zhang for helpful discussions.

REFERENCES

(1) Armand, M.; Tarascon, J. M. *Nature* **2008**, *451*, 652–657.
(2) Tarascon, J. M.; Armand, M. *Nature* **2001**, *414*, 359–367.
(3) Armand, M. *Solid State Ionics* **1994**, *69*, 309–319.
(4) Gray, F., *Solid Polymer Electrolytes*; VCH: New York, 1991.
(5) Wright, P. V. *Br. Polym. J.* **1975**, *7*, 319–327.
(6) Armand, M. B. *Annu. Rev. Mater. Sci.* **1986**, *16*, 245–261.
(7) Meyer, W. H. *Adv. Mater.* **1998**, *10*, 439–448.
(8) Kerr, J. B. Polymeric Electrolytes: An Overview. In *Lithium Batteries*, Nazri, G.-A.; Pistoia, G., Eds.; Kluwer Academic Press: Boston, MA, 2004; pp 574−622.
(9) Eisenberg, A.; Kim, J.-S., *Introduction to Ionomers*; Wiley Interscience: New York, 1998.
(10) Dou, S. C.; Zhang, S. H.; Klein, R. J.; Runt, J.; Colby, R. H. *Chem. Mater.* **2006**, *18*, 4288–4295.
(11) Klein, R. J.; Welna, D. T.; Weikel, A. L.; Allcock, H. R.; Runt, J. *Macromolecules* **2007**, *40*, 3990–3995.
(12) Klein, R. J.; Runt, J. *J. Phys. Chem. B* **2007**, *111*, 13188–13193.
(13) Klein, R. J.; Zhang, S. H.; Dou, S.; Jones, B. H.; Colby, R. H.; Runt, J. *J. Chem. Phys.* **2006**, *124*, 144903.
(14) Register, R. A.; Prud'Homme, R. K. Melt Rheology. In *Ionomers*; Tant, M. R., Mauritz, K. A., Wilkes, G. L., Eds.; Blackie Academic and Professional: London, 1997; pp 208−260.

(15) Colby, R. H.; Zheng, X.; Rafailovich, M. H.; Sokolov, J.; Peiffer, D. G.; Schwarz, S. A.; Strzhemechny, Y.; Nguyen, D. *Phys. Rev. Lett.* **1998**, *81*, 3876–3879.
(16) Green, M. D.; Long, T. E. *Polym. Rev.* **2009**, *49*, 291–314.
(17) Armand, M.; Endres, F.; MacFarlane, D. R.; Ohno, H.; Scrosati, B. *Nat. Mater.* **2009**, *8*, 621–629.
(18) Ohno, H. *Bull. Chem. Soc. Jpn.* **2006**, *79*, 1665–1680.
(19) Ueki, T.; Watanabe, M. *Macromolecules* **2008**, *41*, 3739–3749.
(20) Liu, S.; Liu, W.; Liu, Y.; Lin, J.-H.; Zhou, X.; Janik, M., J.; Colby, R., H.; Zhang, Q. *Polym. Int.* **2010**, *59*, 321–328.
(21) Bennett, M. D.; Leo, D. J. *Sens, Actuators, A: Phys.* **2004**, *115*, 79–90.
(22) Akle, B. J.; Leo, D. J.; Hickner, M. A.; McGrath, J. E. *J. Mater. Sci.* **2005**, *40*, 3715–3724.
(23) Akle, B. J.; Bennett, M. D.; Leo, D. J. *Sens. Actuators, A: Phys.* **2006**, *126*, 173–181.
(24) Duncan, A. J.; Leo, D. J.; Long, T. E. *Macromolecules* **2008**, *41*, 7765–7775.
(25) Duncan, A. J.; Akle, B. J.; Long, T. E.; Leo, D. J. *Smart Mater. Struct.* **2009**, *18*, 104005.
(26) Brown, R. H.; Duncan, A. J.; Choi, J. H.; Park, J. K.; Wu, T. Y.; Leo, D. J.; Winey, K. I.; Moore, R. B.; Long, T. E. *Macromolecules* **2010**, *43*, 790–796.
(27) Eisenberg, A.; Matsura, H.; Yokoyama, T. *J. Polym. Sci., Part A-2: Polym. Phys.* **1971**, *9*, 2131–2135.
(28) Lefelar, J. A.; Weiss, R. A. *Macromolecules* **1984**, *17*, 1145–1148. Weiss, R. A.; Agarwal, P. K.; Lundberg, R. D. *J. Appl. Polym. Sci.* **1984**, *29*, 2719–2734.
(29) Grady, B. P.; Moore, R. B. *Macromolecules* **1996**, *29*, 1685–1690.
(30) Lee, M.; Choi, U. H.; Colby, R. H.; Gibson, H. W. *Chem. Mater.* **2010**, *22*, 5814–5822.
(31) Pedley, A. M.; Higgins, J. S.; Peiffer, D. G.; Burchard, W. *Macromolecules* **1990**, *23*, 1434–1437.
(32) Yarusso, D. J.; Cooper, S. L. *Macromolecules* **1983**, *16*, 1871–1880.
(33) Karayianni, E.; Cooper, S. L. *Ind. Eng. Chem. Res.* **1994**, *33*, 2492–2503.
(34) Roe, R.-J., *Methods of X-ray and Neutron Scattering in Polymer Science*; Oxford University Press: New York, 2000.
(35) Kinning, D. J.; Thomas, E. L. *Macromolecules* **1984**, *17*, 1712–1718.
(36) Leibler, L.; Rubinstein, M.; Colby, R. H. *Macromolecules* **1991**, *24*, 4701–4707.
(37) Vanhoorne, P.; Register, R. A. *Macromolecules* **1996**, *29*, 598–604.
(38) Hara, M.; Sauer, J. A. *Korean J. Chem. Eng.* **1998**, *15*, 353–361.
(39) Rubinstein, M.; Colby, R., H. *Polymer Physics*; Oxford University Press: New York, 2003.
(40) Sangoro, J. R.; Iacob, C.; Serghei, A.; Friedrich, C.; Kremer, F. *Phys. Chem. Chem. Phys.* **2009**, *11*, 913–916.
(41) Kremer, F.; Schönhals, A., *Broadband Dielectric Spectroscopy*; Springer-Verlag: Berlin, 2003.
(42) van Turnhout, J.; Wubbenhorst, M. *J. Non-Cryst. Solids* **2002**, *305*, 50–58.
(43) Wubbenhorst, M.; van Turnhout, J. *J. Non-Cryst. Solids* **2002**, *305*, 40–49.
(44) Fragiadakis, D.; Dou, S.; Colby, R. H.; Runt, J. *J. Chem. Phys.* **2009**, *130*, 064907–11.
(45) Fragiadakis, D.; Dou, S. C.; Colby, R. H.; Runt, J. *Macromolecules* **2008**, *41*, 5723–5728.
(46) Macdonald, J. R. *Phys. Rev.* **1953**, *92*, 4–17.
(47) Sangoro, J. R.; Serghei, A.; Naumov, S.; Galvosas, P.; Karger, J.; Wespe, C.; Bordusa, F.; Kremer, F. *Phys. Rev. E* **2008**, *77*, 051202.
(48) Pajkossy, T. *Solid State Ionics* **2005**, *176*, 1997–2003.
(49) Nakamura, K.; Saiwaki, T.; Fukao, K. *Macromolecules* **2010**, *43*, 6092–6098.
(50) Dyre, J. C.; Maass, P.; Roling, B.; Sidebottom, D. L. *Rep. Prog. Phys.* **2009**, *72*, 046501.
(51) Borodin, O.; Smith, G. D. *Macromolecules* **2006**, *39*, 1620–1629.
(52) Kakihana, M.; Schantz, S.; Torell, L. M. *J. Chem. Phys.* **1990**, *92*, 6271–6277.
(53) Salomon, M.; Xu, M. Z.; Eyring, E. M.; Petrucci, S. *J. Phys. Chem.* **1994**, *98*, 8234–8244.
(54) Schantz, S.; Torell, L. M.; Stevens, J. R. *J. Chem. Phys.* **1991**, *94*, 6862–6867.
(55) Bohmer, R.; Jeffrey, K. R.; Vogel, M. *Prog. Nucl. Magn. Reson. Spectrosc.* **2007**, *50*, 87–174.
(56) Fuoss, R. M.; Kraus, C. A. *J. Am. Chem. Soc.* **1933**, *55*, 2387–2399.
(57) Hojo, M. *Pure Appl. Chem.* **2008**, *80*, 1539–1560.
(58) Barthel, J. M. G.; Krienke, H.; Kuntz, W. *Physical Chemistry of Electrolyte Solutions*; Springer: New York, 1998.
(59) Atorngitjawat, P.; Runt, J. *Macromolecules* **2007**, *40*, 991–996.
(60) Wang, S.-W.; Liu, W.; Colby, R. H. *Chem. Mater.* **2011**, *23*, 1862–1873.
(61) Onsager, L. *J. Am. Chem. Soc.* **1936**, *58*, 1486–1493.
(62) McLin, M. G.; Angell, C. A. *Solid State Ionics* **1992**, *53−6*, 1027–1036.